



# Enhancing the oxidation resistance of Nb-Si based alloys by yttrium addition

Yueling Guo, Lina Jia\*, Huarui Zhang, Fengxiang Zhang, Hu Zhang\*\*

School of Materials Science and Engineering, Beihang University, Beijing, 100191, People's Republic of China



## ARTICLE INFO

**Keywords:**  
Intermetallics  
Aero-engine components  
Microstructure  
Casting  
Oxidation

## ABSTRACT

The effect of yttrium on the microstructure and high-temperature oxidation performance of Nb-15Si-24Ti-4Cr-2Al-2Hf (at.%) alloys was investigated. Alloys containing different yttrium contents were designed, aiming at maximizing the beneficial effect of yttrium addition and avoiding the possible adverse effect of over-doped yttrium. Results showed that Y was primarily partitioned in  $\gamma$ -Nb<sub>5</sub>Si<sub>3</sub>, relative to Nb solid solution (Nbss), Nb<sub>3</sub>Si and  $\alpha$ -Nb<sub>5</sub>Si<sub>3</sub>. Microstructural refinement and oxidation resistance enhancement were achieved by yttrium addition up to 0.3 at.%, accompanied by the transition towards parabolic oxidation kinetics. An adverse effect of over-doped yttrium (0.5 at.% addition) by coarsening the microstructure and deteriorating the oxidation resistance was confirmed. A relatively continuous glassy SiO<sub>2</sub> layer was generated in the oxide scale formed on the Y-containing alloys with enhanced oxidation resistance.

## 1. Introduction

The development of the Nb-Si based alloy family, with increasing temperature capacity relative to current Ni based superalloys, is motivated by the strong need for applications in the hot-sections of both aircraft engines and land-based gas turbines [1–3]. The competitive properties of Nb-Si based alloys are their high melting points (> 1750 °C), relatively lower densities (6.6–7.2 g/cm<sup>3</sup>) and attractive high-temperature stiffness and strength [3–5]. Unfortunately, as a result of their poor oxidation resistance, a balance of targeted properties of Nb-Si based alloys have not been achieved yet.

Nb-Si based alloys typically consist of metallic Nb solid solution (Nbss) and intermetallic Nb<sub>3</sub>Si and/or Nb<sub>5</sub>Si<sub>3</sub>. Silicides are known to possess excellent oxidation resistance, but Nbss typically has a poor oxidation resistance with a larger oxygen solubility and a faster oxygen diffusion rate, which is responsible for the insufficient oxidation resistance of Nb-Si based alloys [6,7]. The formation of non-protective Nb<sub>2</sub>O<sub>5</sub> on Nb-Si based alloys tends to cause large volume expansion and generate considerable growth stress in the oxide scale [7,8]. To protect Nb-Si based alloys from severe oxidation, modified silicide coatings, such as Si-B, Si-Al, Si-Cr and Si-Ge, have been developed [9–12]. The weight gain of Mo-Si-B coating was as low as 0.92 mg/cm<sup>2</sup> after oxidation at 1250 °C for 100 h, ~0.9% of that of a typical Nb-Si based alloy [11]. However, the inherent oxidation resistance of Nb-Si based alloy is also required to survive in case of coating failure.

In addition to coatings, alloying is an effective strategy to enhance

the high-temperature oxidation resistance of Nb-Si based alloys. Examples of this strategy involve Ti, Hf, Cr, Al, Sn, B, Ge, Re and Zr [3,6,13–19]. Ti and Hf additions can promote the formation of a compact and protective oxide scale by reducing the growth stress of oxides during oxidation [19,20]. The diffusivity of oxygen through Nbss is normally suppressed as a result of the synergy of Ti, Cr and Al additions [20]. A sufficient addition of Cr facilitates the formation of Laves Cr<sub>2</sub>Nb phases, which have superior oxidation resistance [21,22]. B and Ge additions have been reported to greatly improve the oxidation resistance of Nb-Si based alloys, by promoting the formation of glassy SiO<sub>2</sub> and thus a more protective oxide scale [23]. The positive effect of yttrium, a rare earth element, on the oxidation resistance of some metals and coatings, including silicide coatings and Mo-Si-B alloys, has been demonstrated [9,24]. The Si-Ge-Y coatings showed finer grain size than the Si-Ge coatings, leading to the improvement in their oxidation resistance by promoting the formation of protective SiO<sub>2</sub> and GeO<sub>2</sub> scale [9]. For Y-containing Mo-Si-B alloys, S. Majumdar et al. [24] found that the Y addition acted to promote the formation of fine yttrium-molybdate phases at the early stages of oxidation, suppress the generation of volatile MoO<sub>3</sub> and facilitate the formation of silica-rich layer with reduced tensile stress. However, the effect of yttrium addition on the microstructure and oxidation resistance of Nb-Si based alloys has been scarcely reported.

Here we investigate the microstructure and the oxidation behavior of Y-containing Nb-Si based alloys. The alloys with the yttrium contents ranging from 0.05 at.% to 0.5 at.% are designed to maximize the

\* Corresponding author.

\*\* Corresponding author.

E-mail addresses: [jialina@buaa.edu.cn](mailto:jialina@buaa.edu.cn) (L. Jia), [zhanghu@buaa.edu.cn](mailto:zhanghu@buaa.edu.cn) (H. Zhang).

beneficial effect of yttrium addition and explore the corresponding high-temperature oxidation kinetics. Meanwhile, we also aim at avoiding the possible adverse effect of excessive Y addition on the oxidation performance. In addition to the oxidation kinetics, microstructural and chemical mechanisms are considered for the improved oxidation resistance of Y-containing alloys. This work potentially provides valuable new compositional input towards the design of high performance Nb-Si based alloys at the elevated temperatures.

## 2. Experimental

The Nb-Si based alloys with different Y contents were synthesized via vacuum non-consumable arc-melting, with the mixture of high-purity niobium, silicon, titanium, chromium, aluminum, hafnium and yttrium. All the raw materials were ultrasonically cleaned and precisely weighed. Nominal compositions of these experimental alloys were Nb-15Si-24Ti-4Cr-2Al-2Hf- $x$ Y (at.%), where  $x = 0, 0.05, 0.1, 0.15, 0.3$  and  $0.5$ , respectively. The Nb-15Si-24Ti-4Cr-2Al-2Hf (at.%) alloy was the reference and denoted as base alloy, while the other five alloys were denoted as 0.05Y alloy, 0.1Y alloy, 0.15Y alloy, 0.3Y alloy and 0.5Y alloy, respectively, according to the Y concentration. Each button was 1.5 kg in weight. The button ingots were remelted five times for the sake of chemical homogeneity.

Oxidation tests were performed in a tube furnace at 1250 °C in static air. All the specimens were cut by electro-discharge machining (EDM) and gradually ground with SiC papers up to 800 grit. Each specimen was placed in a separate alumina crucible during oxidation tests. All the alumina crucibles were heated at 1250 °C for 2 h prior to oxidation. The specimens were removed from the furnace after a certain exposure time. They were weighed together with the crucible using a precision analytical balance (Model CPA225D, Germany) with an accuracy of 0.00001 g. To investigate the initial oxidation behavior of Y-containing Nb-Si based alloys, the 0.3Y alloy was oxidized at 1250 °C for 2 h.

Plate-like and powder samples were used to determine the main phases of the alloy and oxide scales by X-ray diffraction (XRD, D/max-2500, Cu K $\alpha$ ) measurements, respectively. The  $2\theta$  scanning rate was 6°/min. Microstructural and compositional analyses were performed using an electron probe microanalyzer (EPMA, JXA-8230) in the back-scattered electron (BSE) imaging mode and the attached wavelength dispersive spectroscopy (WDS). The average diameter of more than three hundred Nb<sub>5</sub>Si<sub>3</sub> particles in each alloy was measured. To observe the sectional microstructure, the oxidized alloys were mounted with epoxy resin, ground up to 1200# and finally mechanically polished using Fe<sub>2</sub>O<sub>3</sub>/CrO<sub>3</sub> solution. The oxide scale grown on the 0.3Y alloy was examined using a transmission electron microscope (TEM) attached with an energy dispersive X-ray analysis system (EDS). The thin foil for TEM was mechanically thinned to 100  $\mu$ m and finally ion-milled.

## 3. Results

According to the XRD patterns displayed in Fig. 1, the main phases of Nb-15Si-24Ti-4Cr-2Al-2Hf- $x$ Y ( $x = 0, 0.05, 0.1, 0.15, 0.3$  and  $0.5$ , at.%) alloys are Nbss,  $\alpha$ -Nb<sub>5</sub>Si<sub>3</sub> and Nb<sub>3</sub>Si. Additional phases caused by the addition of Y are not detected by the XRD patterns. It is observed that the intensity of  $\alpha$ -Nb<sub>5</sub>Si<sub>3</sub> characteristic peaks are not the same for different alloys, which probably results from the existence of preferred crystal orientations in the plate-like samples used for XRD measurements. Microstructures of these experimental Nb-Si based alloys, taken in the BSE imaging mode, are shown in Fig. 2. There is a trend towards refined microstructure as a result of the addition of Y up to 0.3 at.%. However, the 0.5 at.% addition of Y coarsens the microstructure (Fig. 2f). Higher magnification BSE images displaying their microstructures are shown in Fig. 3. Light grey Nbss, medium grey Nb<sub>3</sub>Si and dark grey  $\alpha$ -Nb<sub>5</sub>Si<sub>3</sub> are observed. All the base and Y-containing alloys show hypoeutectic microstructures, indicated by the formation of primary Nbss dendrites. The solidification process starts with the

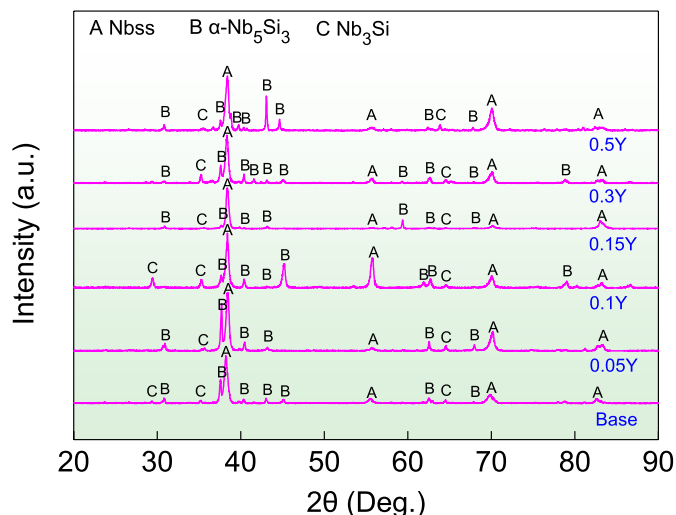


Fig. 1. XRD patterns of the base (without yttrium addition) and yttrium-containing Nb-Si based alloys.

crystallization of primary Nbss, expressed as  $L \rightarrow \text{Nbss} + L_1$ . It is worth noting that  $\gamma$ -Nb<sub>5</sub>Si<sub>3</sub> particles in black contrast are formed in each alloy. They are not detected by the XRD patterns in Fig. 1, probably due to their small volume fraction.

The composition of each phase in the 0.5Y alloy is listed in Table 1. Compared with the Nbss dendrites, Nbss in the eutectic structures is richer for the elements with relatively lower melting temperature (Ti, Cr and Al), which are typically rejected in front of the liquid/solid interface during solidification [25]. The content of Ti in  $\gamma$ -Nb<sub>5</sub>Si<sub>3</sub> (30.04 at.%) is higher than that in  $\alpha$ -Nb<sub>5</sub>Si<sub>3</sub> (17.45 at.%) and Nb<sub>3</sub>Si (18.43 at.%), which suggests Ti may promote the formation of  $\gamma$ -Nb<sub>5</sub>Si<sub>3</sub>. Y is primarily partitioned in  $\gamma$ -Nb<sub>5</sub>Si<sub>3</sub>, as the content of Y in  $\gamma$ -Nb<sub>5</sub>Si<sub>3</sub> is much higher than that in other phases, which is in accordance with the result reported by Chumarev et al. [26].

As shown in Fig. 4, the average diameters of Nb<sub>5</sub>Si<sub>3</sub> particles in the base alloy, 0.05Y alloy, 0.1Y alloy, 0.15Y alloy, 0.3Y alloy and 0.5Y alloy are 8.0  $\mu$ m, 6.9  $\mu$ m, 5.7  $\mu$ m, 3.0  $\mu$ m, 2.3  $\mu$ m, and 19.2  $\mu$ m, respectively. It indicates Nb<sub>5</sub>Si<sub>3</sub> particle size decreases with the Y content up to 0.3 at.%, while over-doped Y (0.5 at.%) results in the coarsening of Nb<sub>5</sub>Si<sub>3</sub> particles.

Fig. 5a shows the weight gain as a function of exposure time for the base and Y-containing alloys at 1250 °C. The weight gain of the experimental alloy after oxidized for 48 h decreases gradually with the content of Y up to 0.3 at.%. Especially, the weight gain of 0.3Y alloy after oxidation testing is as low as 77.0 mg/cm<sup>2</sup>, 43% lower than that of the base alloy (135.1 mg/cm<sup>2</sup>). However, 0.5 at.% Y addition leads to the increase of weight gain to 174.5 mg/cm<sup>2</sup>, ~29% higher than that of the base alloy and 127% higher than that of 0.3Y alloy. This oxidation testing result suggests a proper amount of Y addition (less than 0.3 at.%) improves the oxidation resistance of Nb-Si based alloys, but an excessive addition of Y damages their anti-oxidation property.

The weight of the oxidized alloys shown in Fig. 5a increases rapidly during the first 3 h, but the rate of the weight increase continuously decreases with exposure time. Such oxidation behavior can be described based on a power-law dependence:

$$\Delta m = kt^n \quad (1)$$

where  $\Delta m$  is the weight gain per unit surface area,  $k$  is the oxidation rate constant,  $t$  is the exposure time, and  $n$  is the time exponent to differentiate processes limiting oxide growth. Fig. 5b shows oxidation kinetics of the experimental alloys for Fig. 5a on a log-log scale, and accordingly, the  $k$  and  $n$  values are obtained from the fitting data of Fig. 5b, as tabulated in Table 2. The decrease in time exponent ( $n$ ) with the Y content contained in the alloy is demonstrated, i.e., closer to 0.5

Download English Version:

<https://daneshyari.com/en/article/7988226>

Download Persian Version:

<https://daneshyari.com/article/7988226>

[Daneshyari.com](https://daneshyari.com)